INTERNATIONAL JOURNAL OF PRECISION ENGINEERING AND MANUFACTURING Vol. 15, No. 2, pp. 283-290 FEBRUARY 2014 / 283
DOI: 10.1007/s12541-014-0336-7

Analysis of 5-DOF Motion Errors Influenced by the Guide Rails of an Aerostatic Linear Motion Stage

Gyungho Khim[1], Jeong Seok Oh[1], and Chun Hong Park[1,#]

1 Department of Ultra Precision Machines and Systems, Korea Institute of Machinery and Materials, 156, Gajeongbuk-ro, Yuseong-gu, Deajeon, South Korea, 305-343
Corresponding Author / E-mail: pch657@kimm.re.kr, TEL: +82-42-868-7117, FAX: +82-42-868-7180

KEYWORDS: 5-DOF motion errors, Air bearings, Linear motion stage, Rail form error, Transfer function

This paper presents an estimation method for five-degrees-of-freedom (5-DOF) motion errors, which are influenced by the profiles of guide rails of an aerostatic linear motion stage. The transfer function, which is the relationship between the magnitude of the rail form error and the reaction force of a bearing pad, was introduced to simplify and systematize the estimation of the motion errors. The motion errors were calculated from the equilibrium conditions for the forces and moments of the stage using the geometrical relationships between the bearing pads, the transfer function, and rail form errors. Experimental verification of the rail form error was carried out using a porous aerostatic linear motion stage and the mixed sequential two-probe method. The aerostatic feed table of the experimental stage, on which sensors were mounted, was also used as the feed unit for measuring the rail profiles. The 5-DOF motion errors were estimated from the measured rail form errors using the transfer function method. The estimated results were in good agreement with the experiments.

Manuscript received: July 16, 2013 / Accepted: January 2, 2014

1. Introduction

Recently, the required accuracy for precision equipment, such as machine tools and semiconductor and display processing devices, has become extremely tight. The linear motion stage plays an important role in determining the accuracy of such equipment. However, its accuracy is usually estimated empirically or experimentally in the design process because the designer has no tools for calculating quantitatively the accuracy of the assembled stage. A theoretical and quantitative assessment of the accuracy before fabrication could be quite effective in optimizing the final product.[1,2]

Positioning accuracy is mainly affected by the driving and control elements, whereas the other five-degrees-of freedom (5-DOF) motion errors (vertical and horizontal straightness errors, pitch, yaw, and roll) are largely affected by the rail profile that guides the feed table. Therefore, final finishing process on the rail surface such as scraping or lapping by the skilled workers has been required to satisfy the required motion accuracy in the precision stages. If the motion errors of the stages can be predicted from the rail profile in the design step, the allowable tolerance of the rail form error could be assessed before fabrication, and the time for finishing process could be greatly reduced.

The easiest way to analyze the 5-DOF motion errors is to apply finite element analysis to the entire stage under equilibrium conditions for the forces and moments. However, the model becomes quite cumbersome and complex for 5-DOF, and is difficult to apply to various types of stages. One way to analyze motion errors systematically is to use the transfer function method (TFM).[3,4] This method utilizes the reaction force characteristics of one bearing pad and the geometric relationship between the bearing pads to analyze the relative motion errors between the feed table and rail form error. Therefore, the variation in the reaction forces of multiple bearing pads can be superimposed for the estimation, eliminating the need for a full analysis of the entire stage. The effectiveness of the TFM was verified by estimating the 2-DOF motion errors of linear motion stages in the previous study.[3,4]

In this paper, we extended the TFM to analyze the 5-DOF motion errors of an aerostatic linear motion stage. An analytical model was derived from the equilibrium conditions for the forces and moments. The model included the general case in which the dimension of the vertical bearing pads was different from the horizontal one. The influence of external loads created by the linear motor and ballscrew was ignored because this paper focuses on only the relationship between the feed table and rail form error. This paper deals with an aerostatic linear motion stage in its analysis model. However, our analysis model can also be applied to hydrostatic or linear ball-bearing stages.

The aerostatic linear motion stage with porous pad was fabricated and tested to verify the effectiveness of the analytical model. The mixed sequential two-probe method was applied to measure the rail form errors.[5-7] An aerostatic feed table of the experimental stage, on which the sensors were mounted, was also used as the feed unit for measuring the rail profiles to minimize the measuring error as much as possible. The 5-DOF motion errors were estimated using the measured rail form errors and the TFM; the simulation results were verified by the experimental results.

2. Analytical Model of 5-DOF Motion Errors

2.1 Transfer function

The assumptions for introducing the transfer function are as follows:

1) The dimensions of the bearing pads in the same direction (vertical or horizontal) are the same.
2) The bearing stiffness is constant within a range of rail form error.
3) The rail form error has a continuous profile, i.e., it can be represented as a periodic function.

Fig. 1 shows the movement of a porous air bearing pad along the rail. The motion profile (vertical displacement) $z(x)$ of the pad has the same wavelength, λ, but a different magnitude from the rail form error $e(x)$. h_0 and l represent the average clearance and length of the bearing pad, respectively, and δ is the amplitude of the rail form error. Under the assumption that a bearing stiffness K_z is constant within a range of rail form error, the reaction force $f(x)$ of the pad can be expressed by Eq. (1). $f(x)$ is the reaction force of the bearing pad, assuming that it moves straight along the rail, without any variation in the motion error.

$$K_z \cdot z(x) = f(x) \tag{1}$$

Considering the relationship between the input and output of bearing pad motion in the spatial frequency domain, the reaction force $f(\omega)$, which decides the vertical position of a pad, occurs due to the rail form error $e(\omega)$. This relationship is defined as the transfer function $K(\omega)$ given in Eq. (2).[3,4]

$$K(\omega) = \frac{f(\omega)}{e(\omega)} \tag{2}$$

The transfer function describes the magnitude of the reaction force corresponding to each spatial frequency of the rail form error; i.e., it represents the average effect of motion accuracy with respect to each frequency component.

The transfer function is theoretically calculated using general numerical methods for the air bearings; in this case, the constant bearing clearance is substituted by a sinusoidal form having the appropriate frequency. Fig. 2 shows the model for the porous pad; l and l_w represent the length and width of the porous pad, respectively, p is the pressure in the porous pad and bearing clearance, p_s is the supply pressure, p_a is the ambient pressure, h_0 is the average clearance, and h is the clearance considering the rail form error.

Governing equations, including Darcy's law, the continuity equation of flow, and the Reynolds equation, were used to calculate the pressure distribution of the porous air bearings under the assumption of an

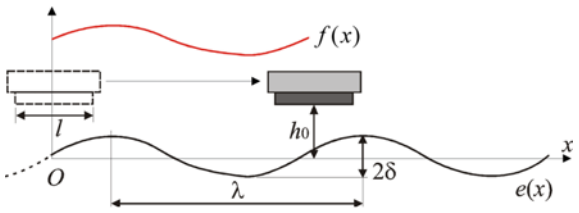

Fig. 1 Response of the bearing reaction force to the sinusoidal profile of the rail

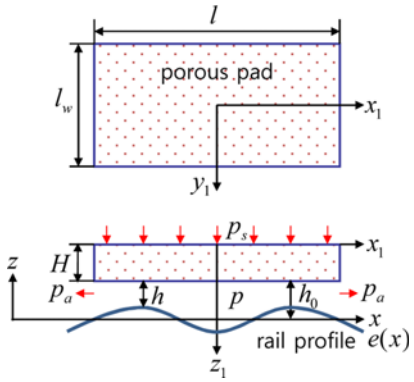

Fig. 2 Modeling of the porous air bearing

isotropic porous material, as shown in Eq. (3).[8-10] The calculations are the same as those used with conventional methods, with the exception of the applied clearance described by the sinusoidal rail form error at each position of the porous pad. The bearing clearance h is given by Eq. (4).

$$\begin{aligned} &\frac{\partial^2 p^2}{\partial x_1^2}+\frac{\partial^2 p^2}{\partial y_1^2}+\frac{\partial^2 p^2}{\partial z_1^2}=0 \\ &\frac{\partial}{\partial x_1}\left(h^3\frac{\partial p^2}{\partial x_1}\right)+h^3\frac{\partial^2 p^2}{\partial y_1^2}-\left|12k_z\frac{\partial p^2}{\partial z_1}\right|_{z_1=H}=0 \end{aligned} \tag{3}$$

$$\begin{aligned} &h(x) = h_0 - e(x) \\ &e(x) = \delta \times \sin(\omega x) \qquad \omega = 2\pi/\lambda \end{aligned} \tag{4}$$

where k_z is the permeability coefficient, and H is the thickness of the porous pad.

The total load capacity W is represented by Eq. (5). The reaction force $f(\omega)$ is calculated from the difference between the maximum and minimum load capacities over one period of the sinusoidal rail form error and has a spatial frequency of ω (Eq. (6)). The magnitude of the rail form error $e(\omega)$ is 2δ, as shown in Fig. 1. Thus, the transfer function $K(\omega)$ is calculated from Eq. (2) using Eq. (6).

$$W(x) = \int_{-l_w/2}^{l_w/2}\int_{-l/2}^{l/2}(p-p_a)dx_1dy_1 \tag{5}$$

$$f(\omega) = \max[W(x)|_{x=0\sim\lambda}] - \min[W(x)|_{x=0\sim\lambda}] \tag{6}$$

2.2 Modeling of 5-DOF motion errors using the transfer function

Fig. 3 shows a model for analyzing the 5-DOF motion errors for the feed table of a linear motion stage. There are multiple rails in the vertical and horizontal directions, under the assumption that the interference

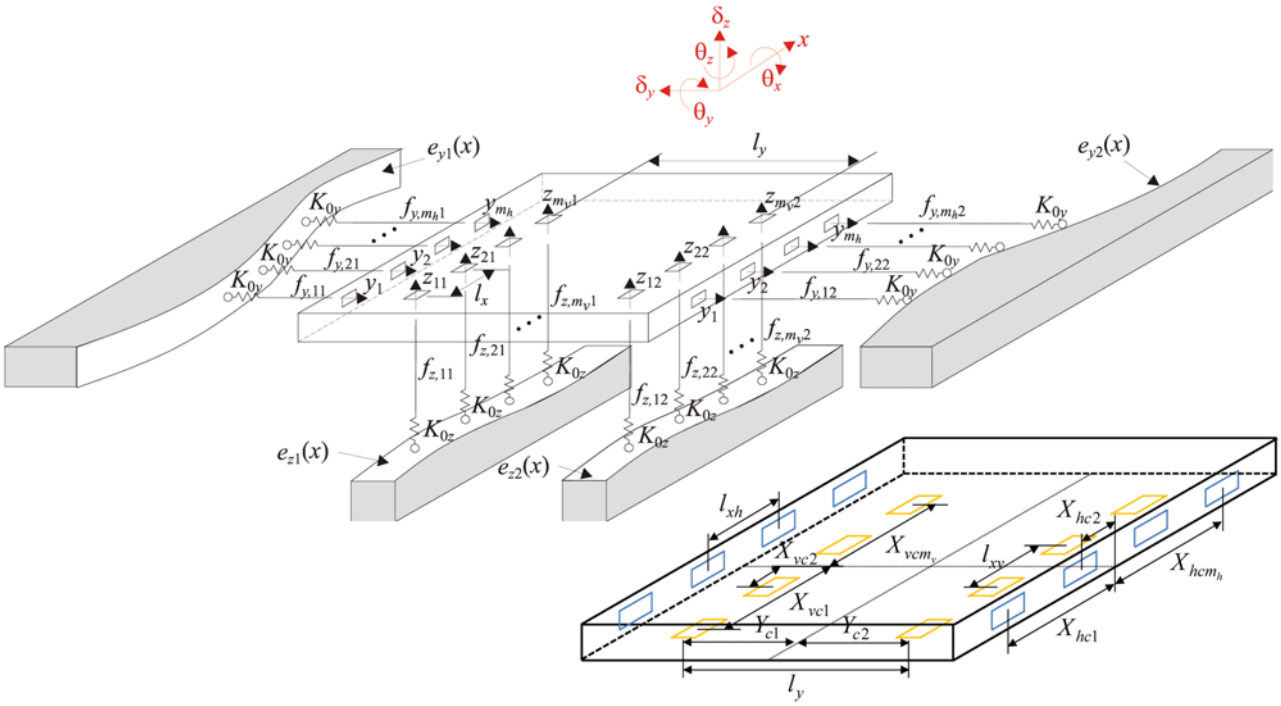

Fig. 3 Analytical model of the feed table for 5-DOF motion errors

from the driving unit or the external load is ignored. The upper side rail and bearing pad are omitted in Fig. 3; however, they can be visualized easily from the relationship between the rail and bearing pad in the horizontal direction. An identical bearing size was assumed for a given direction. The equilibrium equations for the forces and moments for the 5-DOF directions are represented by Eq. (7).

$$\sum_{j}^{n_v}\sum_{i}^{m_v}(f_{z,ij}-K_{0z}z_{ij})=0$$

$$\sum_{j}^{n_v}\sum_{i}^{m_v}\{f_{z,ij}(X_{vci}+\gamma_{vi})-K_{0z}z_{ij}X_{vci}\}=0$$

$$\sum_{j}^{n_v}\sum_{i}^{m_v}(f_{z,ij}Y_{cj}-K_{0z}z_{ij}Y_{cj})+z_c\sum_{j}^{n_h}\sum_{i}^{m_h}(f_{y,ij}-K_{0y}y_{ij})=0 \tag{7}$$

$$\sum_{j}^{n_h}\sum_{i}^{m_h}(f_{y,ij}-K_{0y}y_{ij})=0$$

$$\sum_{j}^{n_h}\sum_{i}^{m_h}\{f_{y,ij}(X_{hci}+\gamma_{hi})-K_{0y}y_{ij}X_{hci}\}=0$$

where $f_{z,ij}$ and $f_{y,ij}$ are the z- and y-direction reaction forces, respectively, caused by the rail form errors at the i,jth pad, z_{ij} and y_{ij} are the pad displacements, K_{0z} and K_{0y} are the stiffness of the pad in the z and y-directions, respectively; m_v and m_h are the number of pads per rail in the vertical(z) and horizontal(y) directions of the x-axis, respectively; n_v and n_h are the number of guide rail surfaces in the vertical and horizontal directions, respectively; Analytical model of Fig. 3 corresponds to the m_v =4, m_h=4, n_v=2, n_h=2; z_c is the height between the rail center and upper surface of the feed table; γ_{vi} and γ_{hi} are the distance between geometric center and moment center of the ith pad in the vertical and horizontal directions, respectively (however, they are ignored in this paper); X_{vci} and X_{hci} are the distances between the pad center and the table center of the vertical(z) and horizontal(y) directions in the x-axis; Y_{cj} is the distance between the pad center and the table center of the vertical directions in the y-axis, represented as Eq. (8); l_{xv} and l_{xh} are the distances between the pads in the vertical and horizontal directions of along the x-axis, respectively; and l_y is the distance between the pads along the y-axis.

$$X_{vci}=l_{xv}\left\{i-\frac{(m_v+1)}{2}\right\},\quad X_{hci}=l_{xh}\left\{i-\frac{(m_h+1)}{2}\right\}$$

$$Y_{cj}=l_y\left\{-j+\frac{(n_v+1)}{2}\right\} \tag{8}$$

Let us suppose δ_z and δ_y are the vertical and horizontal straightness errors, and θ_x, θ_y, and θ_z represent roll, pitch, and yaw errors, respectively, at the table center. Then, the vertical displacement z_{ij} and horizontal displacement y_{ij} caused by the rail form error in the i,jth bearing are expressed by Eq. (9).

$$\begin{aligned} z_{ij}&=\delta_z-X_{vci}\theta_y+Y_{cj}\theta_x \\ y_{ij}&=\delta_y+X_{hci}\theta_z+z_c\theta_x \end{aligned} \tag{9}$$

By substituting Eq. (8) and Eq. (9) into Eq. (7), the matrix equation for the 5-DOF motion errors is expressed by Eq. (10):

$$\begin{bmatrix} 1 & 0 & 0 & 0 & 0 \\ 0 & -A_{0v} & 0 & 0 & 0 \\ 0 & 0 & A_1+C_Kz_c^2 & 0 & C_Kz_c \\ 0 & 0 & 0 & A_{0h} & 0 \\ 0 & 0 & z_c & 0 & 1 \end{bmatrix}\begin{Bmatrix}\delta_z\\ \theta_y\\ \theta_x\\ \theta_z\\ \delta_y\end{Bmatrix}=\begin{bmatrix} 1&0&0&0&0 \\ 0&1&0&0&0 \\ 0&0&1&0&C_Kz_c \\ 0&0&0&1&0 \\ 0&0&0&0&1 \end{bmatrix}\begin{Bmatrix}C_1\\ C_2\\ C_3\\ C_4\\ C_5\end{Bmatrix} \tag{10}$$

where

$$A_{0v}=\frac{(m_v^2-1)l_{xv}^2}{12},\ A_{0h}=\frac{(m_h^2-1)l_{xh}^2}{12},\ A_1=\frac{(n_v^2-1)l_y^2}{12}$$

$$K_A=n_v m_v K_{0z},\ K_B=n_h m_h K_{0y},\ C_K=K_B/K_A$$

$$C_1=\frac{1}{K_A}\sum_j^{n_v}\sum_i^{m_v} f_{z,ij},\ C_2=\frac{1}{K_A}\sum_j^{n_v}\sum_i^{m_v} f_{z,ij}(X_{vci}+\gamma_{vi}),$$

$$C_3=\frac{1}{K_A}\sum_j^{n_v}\sum_i^{m_v} f_{z,ij}Y_{cj}$$

$$C_4=\frac{1}{K_A}\sum_j^{n_h}\sum_i^{m_h} f_{y,ij}(X_{hci}+\gamma_{hi}),\ C_5=\frac{1}{K_A}\sum_j^{n_h}\sum_i^{m_h} f_{y,ij}$$

Because the rail form error is assumed to be periodic, it is represented as a Fourier series in Eq. (11). a_k and b_k are the Fourier coefficients of the corresponding rail, and L is the length of rail.

$$e(x)=\sum_{k=0}^{\infty}\left(a_k\cos\frac{2k\pi}{L}x+b_k\sin\frac{2k\pi}{L}x\right) \tag{11}$$

The reaction forces $f_{z,ij}$ and $f_{y,ij}$ can then be calculated using the transfer function of Eq. (2), as shown in Eq. (12). $K_z(\omega_k)$ and $K_y(\omega_k)$ represent the transfer function in the z and y directions, respectively.

$$f_{z,ij}(x)=\sum_{k=0}^{\infty}K_z(\omega_k)e_{z,jk}(x)$$

$$f_{y,ij}(x)=\sum_{k=0}^{\infty}K_y(\omega_k)e_{y,jk}(x) \tag{12}$$

$$\omega_k=\frac{2k\pi}{L}$$

3. Measurement of Rail Form Errors

3.1 Measurement principle

To predict the 5-DOF motion errors using the proposed analytical model, the rail form errors should be measured first. Fig. 4 shows the porous aerostatic linear motion stage for the experiment. The stage is composed of opposing air bearings with porous pad in the vertical and horizontal directions. Therefore, the rail form errors (e_{z1}, e_{z2}, e_{z3}, e_{z4}, e_{y1}, and e_{y2}) should be measured in this type of configuration.

Custom-designed measuring device for measuring these rail form errors is shown in Fig. 5. To apply the mixed sequential two-probe method,[7] a pair of displacement sensors adjacent to each rail was installed between two porous pads.

Fig. 6(a) and (b) describe the measurement principle based on the mixed sequential two-probe method in the horizontal and vertical directions, respectively.

Displacement sensors A and B were installed in a line on the measuring device, as shown in Setup I of Fig. 6(a). The output signal of the sensors, $R_A(x)$ and $R_B(x)$, are represented by Eqs. (13) and (14), respectively, using the horizontal rail form error $e_{y1}(x)$, the horizontal

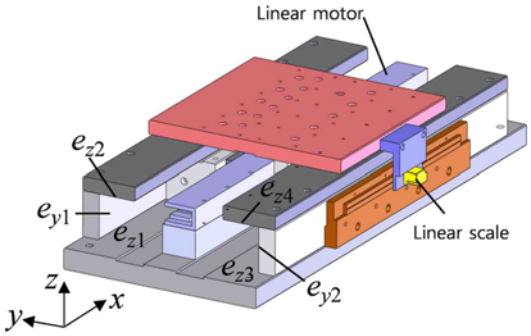

Fig. 4 Porous aerostatic linear motion stage

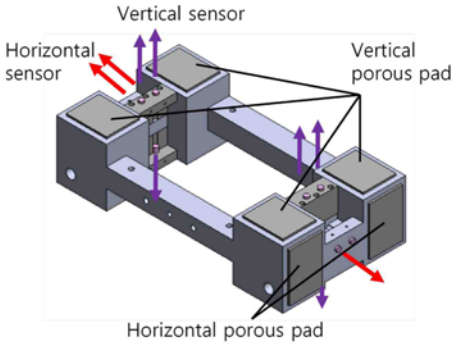

Fig. 5 Custom-designed device for measuring rail form errors

straightness error $\delta_y(x)$, and the angular error (yaw error) $\theta_z(x)$ of the measuring device. The displacement difference between two adjacent sensors (A and B) was compensated for by considering the angular error of the measuring device.

$$R_A(x_i)=e_{y1}(x_i)+\delta_y(x_i) \tag{13}$$

$$R_B(x_i)=e_{y1}(x_{i+1})+\delta_y(x_i)+l_x\cdot\theta_z(x_i) \tag{14}$$

$$R_A(x_{i+1})=e_{y1}(x_{i+1})+\delta_y(x_{i+1}) \tag{15}$$

From Eqs. (13)-(15), the rail form error $e_{y1}(x)$ and the horizontal straightness error $\delta_y(x)$ of the measuring device can be expressed by Eqs. (16) and (17), respectively.

$$e_{y1}(x_{i+1})=e_{y1}(x_i)-R_A(x_i)+R_B(x_i)-l_x\cdot\theta_z(x_i) \tag{16}$$

$$\delta_y(x_{i+1})=\delta_y(x_i)+R_A(x_{i+1})-R_B(x_i)+l_x\cdot\theta_z(x_i) \tag{17}$$

where $e_{y1}(x_0)=0$, and $\delta_y(x_0)=0$.

If we use three sensors with an additional sensor C for the second rail (Setup III in Fig. 6(a)), then the rail form error $e_{y2}(x)$ can be calculated from the output, $R_c(x)$, of Sensor C, and the horizontal straightness error $\delta_y(x)$, as shown in Eq. (18).

$$e_{y2}(x_i)=R_C(x_i)+\delta_y(x_i) \tag{18}$$

Using a similar approach to that for Setup I, with Sensors C and D for the second rail (Setup II in Fig. 6(a)), the rail form error $e_{y2}(x)$ and

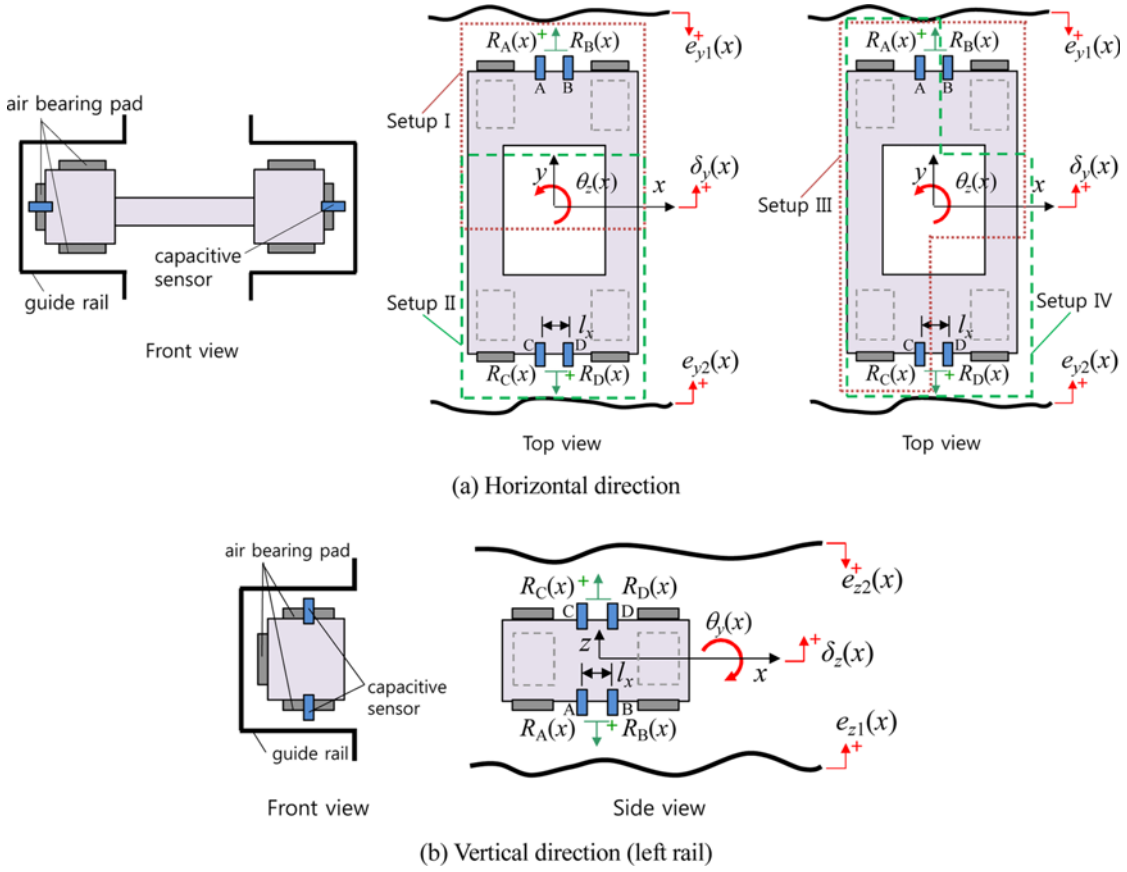

Fig. 6 Measurement principle for rail form errors

horizontal straightness error $\delta_y(x)$ are given by Eqs. (19) and (20).

$$e_{y2}(x_{i+1}) = e_{y2}(x_i) - R_C(x_i) + R_D(x_i) + l_x \cdot \theta_z(x_i) \tag{19}$$

$$\delta_y(x_{i+1}) = \delta_y(x_i) - R_C(x_{i+1}) + R_D(x_i) + l_x \cdot \theta_z(x_i) \tag{20}$$

where $e_{y2}(x_0) = 0$, and $\delta_y(x_0) = 0$.

Additionally, the rail form error $e_{y1}(x)$ can also be calculated from the output $R_A(x)$ of Sensor A and the horizontal straightness error $\delta_y(x)$ with measurement Setup IV in Fig. 6(a), which is expressed by Eq. (21).

$$e_{y1}(x_i) = R_A(x_i) - \delta_y(x_i) \tag{21}$$

The rail form error $e_{y1}(x)$ is obtained from Setup I or IV, whereas the rail form error $e_{y2}(x)$ is calculated from Setup II or III. The horizontal straightness error $\delta_y(x)$ is obtained from Setups I or II. Therefore, the measuring algorithm for the rail form errors can be verified by comparing these two results, which are independently obtained with different setups.

A vertical rail has four rail form errors (i.e., the upper and lower rail form errors for the left and for the right rails), as shown in Fig. 4. The measurement and verification methods are the same as those used for the horizontal rail.

3.2 Experimental setup

Fig. 7 shows the experimental setup for measurement of rail form errors. A rotary motor and a wire rope system were used to move the measuring device at a constant speed of 5 mm s^{-1} via a Delta Tau controller and Copley drive system. A counterbalance was installed to maintain constant tension on the wire rope. A 24-bit analog-to-digital (A/D) board (Dewetron Dewe-43) and capacitance sensors (Lion Precision C6-D, 1-nm resolution) were used to measure the rail profiles. A laser interferometer (HP5529A) was installed to measure the angular error of the measuring device. Figs. 8 and 9 show a photograph of the measuring device and the entire experimental setup, respectively. Table 1 provides the specifications for the measuring devices used in the experiment.

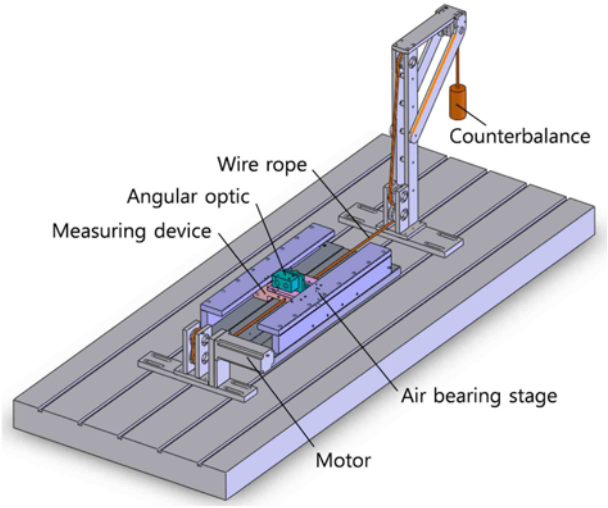

Fig. 7 Schematic diagram of the experimental setup

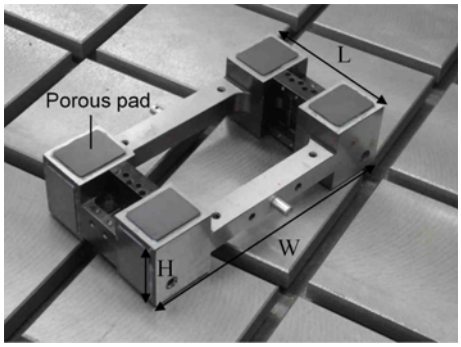

Fig. 8 Photograph of the measuring device

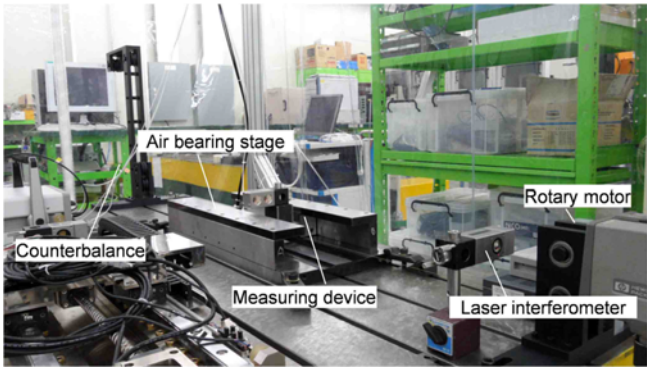

Fig. 9 Photograph of the experimental setup

Table 1 Specifications for the measuring devices

Porous air bearing	Vertical pad (mm)	four double pads, 35×43×5
	Horizontal pad (mm)	two double pads, 35×51×5
	Permeability coefficient (m^2)	7.7×10^{15}
	Supply pressure (Pa)	4×10^5
	Average clearance (μm)	10
Measuring device	Dimension (mm)	130(L)×244(W)×65(H)
	Distance between two sensors (mm)	15

3.3 Measurement results for rail form errors

Fig. 10 shows the rail form errors measured using the proposed method in the horizontal and vertical directions. The amplitudes of the rail form errors are e_{y1}=4.67 and e_{y2}=1.06 μm for the horizontal rails and e_{z1}=1.16, e_{z2}=1.17, e_{z3}=2.24, e_{z4}=2.47 μm for the vertical rails. The direction of the rail form error coincides with Fig. 6.

The rail form errors $e_{y1}(x)$, $e_{y2}(x)$ and the horizontal straightness error $\delta_y(x)$ of the measuring device can be obtained by two different methods, as mentioned earlier in Section 3.1. Fig. 11 shows the comparison results of $e_{y1}(x)$, $e_{y2}(x)$, and $\delta_y(x)$ obtained from the different setups, which were in good agreement with each other. Thus, the proposed algorithm was effective in its ability to measure rail form error.

4. Estimation and Verification of the 5 DOF Motion Errors

The experimental setup for measuring 5-DOF motion errors is the same as that for the rail form error measurement, as shown in Fig. 7.

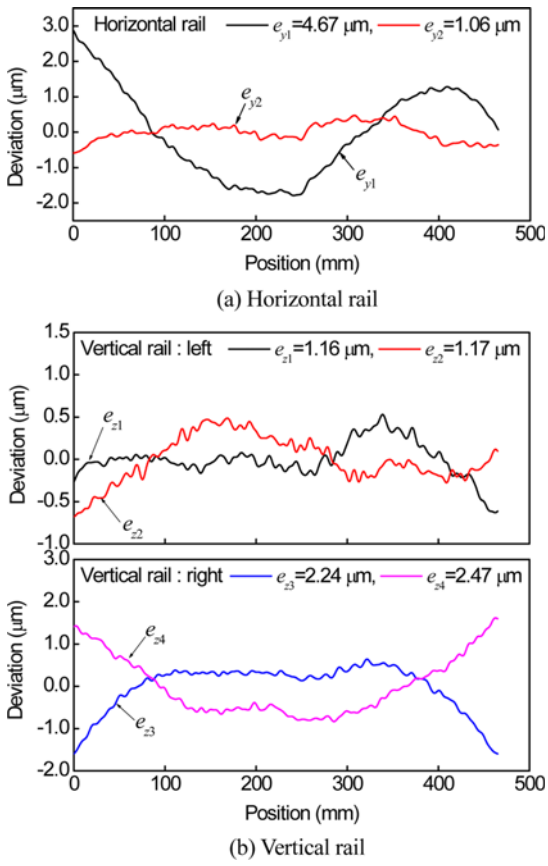

(a) Horizontal rail

(b) Vertical rail

Fig. 10 Measurement results for the rail form errors

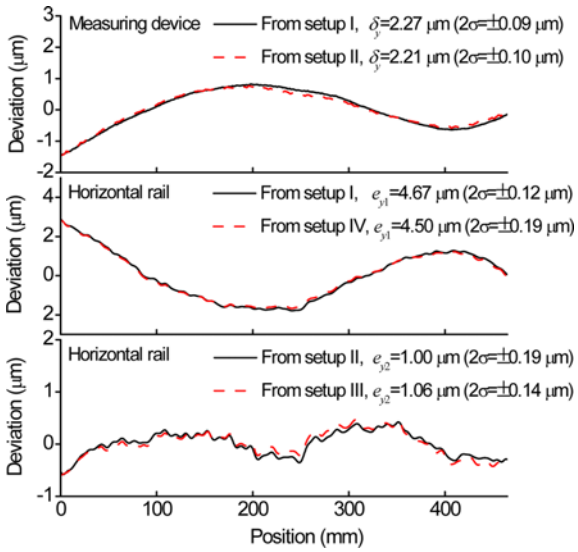

Fig. 11 Verification of the rail form errors

The measuring device takes the role as the feed table as well as the measuring device for the rails. Therefore, an additional feed table, motor, and scale are not required. Additionally, the influence of the rail form errors on the 5-DOF motion errors can be precisely observed because there is no external load caused by linear motor or ballscrew.

The transfer function must be calculated to predict the 5-DOF motion errors. The bearing reaction force can be obtained from Eqs. (3)-(6) for the porous pad of Table 1. From this, the transfer function

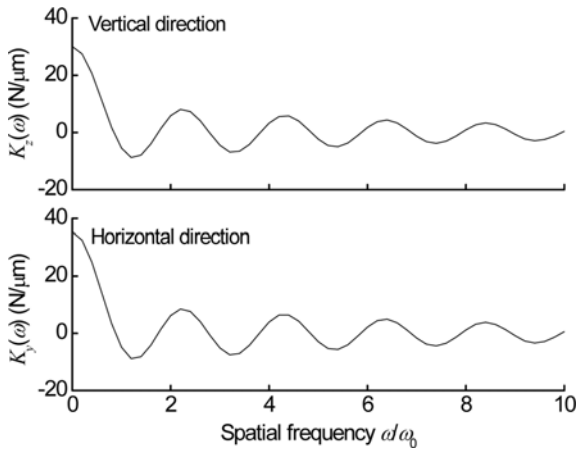

Fig. 12 Calculated transfer function

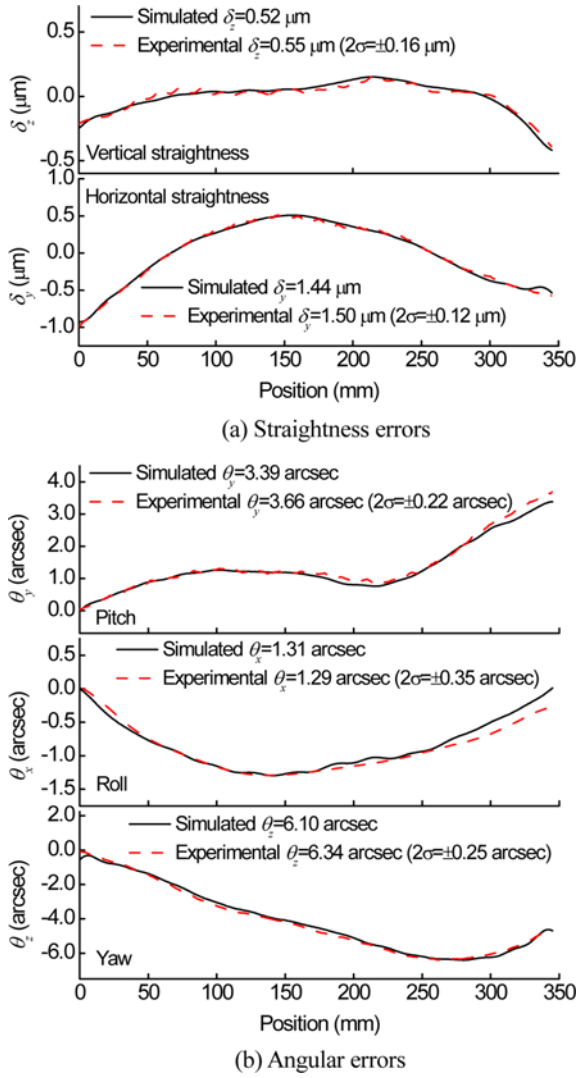

Fig. 13 Comparison between simulated and experimental results

can be determined using Eq. (2).

Fig. 12 shows the calculated transfer function in the vertical and horizontal directions. A reference spatial frequency $\omega_0(=2\pi/l)$ is assigned to a length of the porous pad. The transfer function $K(0)$ at $\omega=0$ corresponds to the static stiffness of the bearing. The 5-DOF motion errors were theoretically estimated from the transfer function and measured rail form errors.

The horizontal and vertical straightness errors of the feed table were measured using the mixed sequential two-probe method, as shown in Fig. 6. With this setup, the rail form error and straightness error (linear motion error of the measuring device) were simultaneously measured. The vertical straightness error was obtained from the left and right rails on both sides. Thus, the vertical straightness error in the center was averaged from these two values. Yaw and pitch errors were measured with a laser interferometer (HP5529A). The roll error was measured using an electronic level meter (Mahr 832F).

Fig. 13 presents the comparison results between simulated and experimental data in the 5-DOF motion errors. The experiment was carried out five times, and results were averaged. The results show that the simulated motion errors were in good agreement with the experiment; this was attributed to using the measuring device for the rail form errors as a feed table for the stage. Therefore, there were no critical error sources in measuring the rail form errors or motion errors.

5. Conclusions

In this paper, an estimation method for the 5-DOF motion errors was introduced for an aerostatic linear motion stage, and its effectiveness was verified by experiment. The motion errors were predicted from the rail form errors using the proposed TFM. The measuring device designed to measure the rail form errors was also used as the feed table for the aerostatic linear motion stage to minimize measuring error. Thus, the rail form errors were simultaneously measured with the straightness errors of the feed table using the mixed sequential two-probe method. The measured rail form errors were verified by comparing the results obtained from several different setups. Finally, the estimated 5-DOF motion errors were compared with the measured motion errors. From the experimental results, we confirmed that the proposed method was very effective in its ability to estimate the 5-DOF motion errors in a linear motion stage.

REFERENCES

1. Altintas, Y., Brecher, C., Weck, M., and Witt, S., "Virtual Machine Tool," CIRP Annals - Manufacturing Technology, Vol. 54, No. 2, pp. 115-138, 2005.

2. Oh, J. S., Khim, G., Park, C. H., Chung, S. C., Lee, S. K., and Kim, S. J., "Accuracy Simulation of the Precision Linear Motion Systems," Journal of Korean Society of Precision Engineering, Vol. 28, No. 3, pp. 275-284, 2011.

3. Shamoto, E., Park, C. H., and Moriwaki, T., "Analysis and Improvement of Motion Accuracy of Hydrostatic Feed Table," CIRP Annals - Manufacturing Technology, Vol. 50, No. 1, pp. 285-290, 2001.

4. Khim, G., Park, C. H., Shamoto, E., and Kim, S. W., "Prediction and Compensation of Motion Accuracy in a Linear Motion Bearing Table," Precision Engineering, Vol. 35, No. 3, pp. 393-399, 2011.

5. Gao, W. and Kiyono, S., "High Accuracy Profile Measurement of a Machined Surface by the Combined Method," Measurement, Vol. 19, No. 1, pp. 55-64, 1996.

6. Tanaka, H. and Sato, H., "Extensive Analysis and Development of Straightness Measurement by Sequential-Two-Points Method," Journal of Engineering for Industry, Vol. 108, No. 3, pp. 176-182, 1986.

7. Oh, J. S., Khim, G., Oh, J. S., and Park, C. H., "Precision Measurement of Rail form Error in a Closed Type Hydrostatic Guideway," Int. J. Precis. Eng. Manuf., Vol. 13, No. 10, pp. 1853-1859, 2012.

8. Singh, K. C. and Rao, N. S., "Static Characteristics of Aerostatic Porous Rectangular Thrust Bearings," Wear, Vol. 77, No. 2, pp. 229-236, 1982.

9. Kwan, Y. B. P. and Corbett, J., "Porous Aerostatic Bearings - an Updated Review," Wear, Vol. 222, No. 2, pp. 69-73, 1998.

10. Wu, K. H. and Cusano, C., "Analysis of Externally Pressurized, Double-Pad, Gas Porous Thrust Bearing," Journal of Lubrication Technology, Vol. 105, No. 1, pp. 113-119, 1983.